



1 **Meteorological characteristics of severe ozone pollution events in**
2 **China and their future predictions**

3

4

5

6 Yang Yang^{1*}, Yang Zhou², Hailong Wang³, Mengyun Li¹, Huimin Li¹, Pinya Wang¹, Xu Yue¹,

7

Ke Li¹, Jia Zhu¹, Hong Liao¹

8

9

10 ¹Joint International Research Laboratory of Climate and Environment Change, Jiangsu Key

11 Laboratory of Atmospheric Environment Monitoring and Pollution Control, Jiangsu

12 Collaborative Innovation Center of Atmospheric Environment and Equipment Technology,

13 School of Environmental Science and Engineering, Nanjing University of Information

14 Science and Technology, Nanjing, Jiangsu, China

15 ²Shanghai Baoshan Meteorology Bureau, Shanghai, China

16 ³Atmospheric Sciences and Global Change Division, Pacific Northwest National Laboratory,

17

Richland, WA, USA

18

19

20

21

22 *Correspondence to yang.yang@nuist.edu.cn



23 **Abstract**

24 Ozone (O₃) has become one of the most concerning air pollutants in China in recent
25 decades. In this study, based on surface observations, reanalysis data and global atmospheric
26 chemistry model simulations, meteorological characteristics conducive to severe O₃ pollution
27 in various regions of China are investigated, and their historical changes and future trends are
28 analyzed. During the most severe O₃ pollution months over the North China Plain (NCP) and
29 Yangtze River Delta (YRD), the chemical production of O₃ is enhanced under the hot and dry
30 conditions, while the regional transport is the main reason causing the severe O₃ pollution over
31 Sichuan Basin (SCB) and Pearl River Delta (PRD) during the severe polluted months. Over
32 the last four decades, the frequencies of high temperature and low relative humidity conditions
33 increased in 2000-2019 relative to 1980-1999, indicating that O₃ pollution in both NCP and
34 YRD became more frequent under the historical climate change. In SCB and PRD, the
35 occurrence of atmospheric circulation patterns similar to those during the polluted months
36 increased, together with the more frequent hot and dry conditions, contributing to the increases
37 in severe O₃ pollution in SCB and PRD during 1980–2019. In the future (by 2100), the
38 frequencies of months with anomalous high temperature show stronger increasing trends in the
39 high forcing scenario (SSP5-8.5) compared to the sustainable scenario (SSP1-2.6) in China. It
40 suggests that high anthropogenic forcing will not only lead to slow economic growth and
41 climate warming, but also likely result in environmental pollution issues.



42 **1. Introduction**

43 Tropospheric ozone (O_3), one major air pollutant, is formed in photochemical reactions of
44 nitrogen oxides (NO_x) and volatile organic compounds (VOCs) when exposed to sunlight
45 (Finlayson-Pitts and Pitts, 1997; Silman, 1999). Enhanced O_3 pollution harms ecosystems and
46 human health (Fleming et al., 2018; Maji et al., 2019) by reducing crop yields (Ainsworth et
47 al., 2012; Mills et al., 2018) and aggravating cardiopulmonary disease (Ebi and McGregor,
48 2008; Liu et al. 2018). In recent years, near-surface ozone concentrations in many regions of
49 China have been increasing considerably (Verstraeten et al., 2015; Cheng et al., 2019; Zhang
50 et al., 2020, Li et al., 2019; Lu et al., 2018; Silver et al., 2018; Yin et al., 2019, Lu et al., 2020).
51 Lu et al. (2020) revealed that the daily maximum of 8-h average O_3 concentration (MDA8- O_3)
52 in China increased by 2.4 ppb per year (5.0% relative to the average) during April–September
53 over 2013–2019.

54 In addition to emissions, O_3 concentrations are influenced by meteorological factors such
55 as temperature, relative humidity, solar radiation, and winds (Mott et al., 2005; Fu and Tian,
56 2019; Gong and Liao, 2019; Li et al., 2019, 2020; Le et al., 2020; Zhao et al., 2020). Typically,
57 strong solar radiation, high surface air temperatures, and low relative humidity are conducive
58 to photochemical production of O_3 , causing a raise of O_3 concentration (Peterson and Flowers,
59 1977; Xu, et al., 2011; Coates et al., 2016; Li et al., 2020; Dang et al., 2021). Wind speed is
60 negatively correlated with surface O_3 because low wind speed facilitates the accumulation of
61 O_3 upon production (Zhang et al., 2015; Wang et al., 2017; Liu and Wang, 2020). Han et al.
62 (2020) explored the impacts of various meteorological factors on the daily variation of summer
63 surface O_3 in eastern China based on a multiple linear regression method and suggested that



64 relative humidity is the primary factor affecting O₃ concentration in central and south parts of
65 eastern China, while temperature is the most important factor governing O₃ concentration in
66 north of eastern China. Gong and Liao (2019) reported that the meteorological characteristics
67 of O₃ pollution events in North China during 2014–2017 were the high daily maximum
68 temperature, low relative humidity, abnormal southerly winds and high pressure at 500 hPa.
69 These findings emphasize that meteorological factors play a crucial role in regulating O₃
70 pollution in China.

71 Atmospheric circulation patterns affect O₃ concentrations over China through changing
72 meteorological factors (Yang et al, 2014; Zhao and Wang, 2017; Shu et al., 2019; Dong et al.,
73 2020; Zhou et al., 2022). Zhao and Wang (2017) examined the influence of the Western Pacific
74 Subtropical high (WPSH) on O₃ over eastern China based on observations and reanalysis data
75 from 2014 to 2016. They found that stronger WPSH enhanced the moisture transport to
76 southern China, which was detrimental to the photochemical reaction of O₃, leading to a
77 decrease in surface O₃ concentration in southern China, whereas O₃ concentrations in northern
78 China increased under the stronger WPSH related to the dry and hot conditions favoring O₃
79 production. On the basis of observational O₃ data and ERA5 reanalysis data during 2014–2018,
80 Dong et al. (2019) analyzed the impact of synoptic patterns on summertime O₃ pollution in the
81 North China Plain and revealed that the most severe O₃ pollution weather pattern is associated
82 with anomalous southwesterly winds, which carry dry, warm air from inland southern China
83 to the North China Plain and favor the chemical production of O₃. Zhou et al. (2022) explored
84 the impacts of Asian summer monsoon on the interannual variation of O₃ concentrations based
85 on surface measurements and GEOS-Chem model simulations. They showed that the East



86 Asian summer monsoon strength was positively correlated with O₃ concentration in south-
87 central China and South Asian summer monsoon has complex effects on O₃ pollution in China,
88 mainly through changing transboundary transport related to large-scale circulations.

89 As mentioned above, previous studies have examined the meteorological characteristics
90 of O₃ pollution in limited regions in China. In this study, the meteorological characteristics
91 conducive to severe O₃ pollution in several polluted areas of China, including the North China
92 Plain (NCP), Yangtze River Delta (YRD), Sichuan Basin (SCB), and Pearl River Delta (PRD),
93 are investigated based on the observed surface O₃ concentrations, reanalysis data, and GEOS-
94 Chem model simulations. Besides, the contributions from various chemical and physical
95 processes inducing regional O₃ pollution are quantified using an integrated process rate (IPR)
96 analysis method. Moreover, variations of future meteorological patterns leading to severe O₃
97 pollution in China are presented under the sustainable and high forcing scenarios according to
98 the multi-model data from the Coupled Model Intercomparison Project Phase 6 (CMIP6).

99 **2. Methods**

100 **2.1 Surface ozone observations and meteorological reanalysis**

101 Hourly surface O₃ concentrations are obtained from the Ministry of Ecology and
102 Environment (MEE) of China. The observational network was established in 2013 with 450
103 monitoring sites and increased to 1,500 monitoring sites by 2019, covering about 360 cities in
104 China. MDA8-O₃ are calculated based on hourly O₃ concentrations from April-September
105 during 2013 to 2020. In this study, O₃ pollution days are defined as the days when MDA8-O₃
106 exceeds 160 µg m⁻³ according to the China National Ambient Air Quality Standard (GB3095-
107 2012).



108 The meteorological fields are taken from the European Centre for Medium-Range
109 Weather Forecasts (ECMWF) ERA5 monthly reanalysis dataset during 1980–2020, with a
110 horizontal resolution of $0.25^\circ \times 0.25^\circ$. To explore the meteorological characteristics that are
111 conducive to O_3 pollution, sea level pressure (SLP), geopotential height (GPH) at 500 hPa,
112 wind fields at 850 hPa and 500 hPa, temperature at 2m (T2m) and surface relative humidity
113 (RH) are adopted, which can have significant impacts on O_3 variations in China (Jiang et al.,
114 2020; Dong et al., 2020; Le et al., 2020).

115 **2.2 GEOS-Chem model simulations**

116 O_3 concentrations and the related chemical and physical processes causing O_3 variations
117 over 1981–2020 are simulated in the global atmospheric chemistry model GEOS-Chem
118 (version V12.9.3), driven by the Modern-Era Retrospective analysis for Research and
119 Application, Version 2 (MERRA-2). Simulations are performed on 47 vertical layers from
120 surface to 0.01 hPa, and a horizontal grid of 2° latitude \times 2.5° longitude. GEOS-Chem model
121 incorporates a fully coupled O_3 - NO_x -hydrocarbon-aerosol chemical mechanism (Pye et al.,
122 2009; Mao et al., 2013; Sherwen et al., 2016). Boundary-layer mixing uses a non-local scheme
123 (Lin and McElroy, 2010), and stratospheric O_3 chemistry employs the linearized O_3
124 parameterization (LINOZ) (McLinden et al., 2000).

125 Global anthropogenic aerosol and precursor gas emissions driving the simulations are
126 from the Community Emissions Data System (CEDS, Hoesly et al., 2018) and biomass burning
127 emissions are from the Global Fire Emissions Database, Edition 4 (GFED4, Van der Werf et
128 al., 2017). VOCs emissions from biogenic sources are provided offline by the Model of
129 Emissions of Gases and Aerosols from Nature version 2.1 (MEGAN V2.1, Guenther et al.,



130 2012). Lightning and soil emissions are specified in the model (Hudman et al., 2012; Ott et al.,
131 2010). Anthropogenic emissions in China are updated with the Multi-resolution Emission
132 Inventory (MEIC), a localized emission dataset for China. Anthropogenic, biomass burning,
133 biological and other natural emissions are kept at 2017 level during the simulations, so as to
134 eliminate the influence of emission changes on the interannual variation and trends of O₃.
135 Simulated O₃ distributions with the same configuration in GEOS-Chem have been extensively
136 evaluated in many studies, and the model has been reported to capture O₃ concentrations well
137 in China (e.g., Li et al., 2019; Lu et al., 2019; Ni et al., 2018).

138 **2.3 CMIP6 multi-model simulations**

139 The multi-model simulations from historical and the Scenario Model Intercomparison
140 Project (ScenarioMIP) in CMIP6 are used to analyze the historical variations and future trends
141 of meteorological conditions conducive to severe O₃ pollution. Two different future scenarios
142 of the Shared Socioeconomic Path (SSPs) are applied, including the sustainable scenario
143 (SSP1-2.6) and the high forcing scenario (SSP5-8.5). Totally simulations from 13 models
144 (ACCESS-CM2, ACCESS-ESM1-5, CAS-ESM2-0, CMCC-CM2-SR5, CMCC-ESM2,
145 FGOALS-f3-L, FGOALS-g3, GFDL-ESM4, INM-CM4-8, INM-CM5-0, IPSL-CM6A-LR,
146 MPI-ESM1-2-HR, MPI-ESM1-2-LR) are analyzed in this study.

147 **3. Results**

148 **3.1 Meteorological characteristics conducive to regional ozone pollution**

149 To investigate the relationship between meteorological conditions and regional O₃
150 pollution in China, the frequencies of O₃ pollution days from April to September during 2013–
151 2020 are calculated for Beijing, Shanghai, Chengdu and Guangzhou, representing the typical



152 four polluted regions in China (i.e., NCP, YRD, SCB and PRD) (Figure 1). Observational data
153 show the highest frequencies of O₃ pollution days in June 2018, July 2017 and September 2019
154 in Beijing, Shanghai and Guangzhou, with pollution days up to 22, 20 and 19 days per month,
155 respectively. Variations in O₃ concentration in the real world are driven by changes in both
156 meteorological factors and emissions. With fixed emissions, the positive anomalies of near-
157 surface O₃ concentrations over NCP, YRD and PRD during their most polluted months can also
158 be reproduced by the GEOS-Chem model (Figure 2), suggesting that the O₃ pollutions during
159 the most polluted months over NCP, YRD and PRD are likely attributable to the anomalies of
160 meteorological conditions. In the top three O₃ polluted months in Chengdu, only in July 2015
161 the higher concentrations than the long-term averages can be captured by the simulations with
162 fixed emissions. Therefore, in this study, we focus on the meteorological characteristics in June
163 2018, July 2017, July 2015 and September 2019, that were conducive to the severe O₃ pollution
164 over NCP, YRD, SCB and PRD, respectively.

165 When O₃ pollution was the most severe over NCP in June 2018, an anomalous high
166 pressure occurred at 500 hPa over NCP (Fig. 3b), relative to the 40-year climatological
167 averages from 1980 to 2019, leading to positive T2m anomalies near the surface (Fig. 3c).
168 Anomalous lows located over northeastern China and northwestern Pacific (Fig. 3a) and the
169 associated anomalous northerly winds prevent the moisture moving from the ocean to NCP,
170 causing negative RH anomalies over NCP (Fig. 3d). The meteorological conditions with the
171 high T2m and low RH are favorable for the photochemical production of O₃. When the most
172 severe O₃ pollution occurred in July 2017, YRD was dominated by anomalous high pressure
173 in the lower and middle troposphere (Figs. 4a and 4b). Under the control of high pressure, the



174 meteorological conditions (e.g., high T2m and low RH) enhance the photochemical production
175 of O₃ (Figs. 4c and 4d). In the O₃ pollution event of SCB in July 2015, the negative T2m
176 anomaly is not conducive to the O₃ production (Fig. 5c), although the RH was low (Fig. 5d).
177 Meanwhile, the anomalous low over eastern China and northwestern Pacific in the middle
178 troposphere favors regional O₃ transport from the polluted source region over eastern China to
179 SCB (Fig. 5b) and the anomalous high over central-western China is conducive to the vertical
180 transport of upper tropospheric O₃ down to the lower troposphere (Fig. 5a). For the PRD in
181 September 2019, the anomalous high covering almost the entire China along with the
182 anomalous low over East China Sea generates northerly wind anomalies in the lower
183 troposphere over eastern China, which tend to transport polluted air from northern China and
184 weaken the inflow of oceanic clean air (Fig. 6). The temperature increase is much more
185 significant in the upwind regions as compared to PRD, suggesting that the strong regional
186 transport could be the primary reason causing this severe O₃ pollution event of PRD.

187 **3.2 Physical and chemical mechanisms leading to regional ozone pollution**

188 To further explore the mechanisms of meteorological changes leading to the severe O₃
189 pollution over the four typical polluted regions in China, contributions of individual chemical
190 and physical processes to O₃ variations are quantified based on the IPR analysis from GEOS-
191 Chem simulations and summarized in Table 1.

192 Consistent with the meteorological anomalies analyzed above, high temperature and low
193 RH meteorological conditions in NCP are conducive to the photochemical production of O₃.
194 During the polluted month over NCP, the chemical production of tropospheric O₃ is higher than
195 the long-term average by 2.36 Gg day⁻¹, while the horizontal transport also contributes to the



196 increase in O_3 mass by 1.58 Gg day^{-1} (Table 1). Due to the enhanced northwesterly winds, the
197 import of O_3 mass from the north and east of NCP was increased by 1.80 and 0.62 Tg,
198 respectively (Table 2). In YRD, the chemical production (2.38 Gg day^{-1}) is also the dominant
199 process that drives the O_3 concentration increase during the severe polluted month, associated
200 with the warm and dry conditions. Therefore, the anomalous chemical production is the major
201 process that induced O_3 pollution in NCP and YRD during the severe polluted months.

202 Different from NCP and YRD, horizontal transport is the main process that caused O_3
203 pollution in SCB and PRD during the severe polluted months. It contributes to the rate of
204 increase in O_3 mass by 5.10 and 6.67 Gg day^{-1} , respectively, over SCB and PRD, while other
205 processes tend to decrease the O_3 mass (Table 1). Due to the anomalous northerly winds over
206 SCB, more O_3 is transported into SCB from north (by 4.02 Tg), and the anomalous
207 northeasterly winds enhance the O_3 transport from the north and east of PRD by 1.97 and 1.09
208 Tg, respectively, leading to the increase in O_3 concentrations over SCB and PRD during the
209 severe polluted months relative to the climatological averages (Table 2).

210 **3.3 Historical and future changes in the meteorological conditions**

211 O_3 pollution has deteriorated in China during recent decades, which could be related to
212 the changes in meteorological conditions. Time series of T2m and RH anomalies in the polluted
213 months during the 1980–2019 and frequencies of high T2m and low RH months during 1980–
214 1999 and 2000–2019 over the four polluted regions in China based on ERA5 reanalysis data
215 are shown in Figure 7. Due to climate change, both the high temperature and low RH conditions
216 in NCP, YRD, SCB and PRD all increased during the past four decades (2000-2019 versus
217 1980-1999). Based on the analysis showing that chemical production is the dominant process



218 of severe O₃ pollution in NCP and YRD, the increases in the frequency of high temperature
219 and low RH indicate that severe O₃ pollution in both NCP and YRD has become more frequent
220 under the historical climate change. In SCB and PRD, the severe O₃ pollution is more related
221 to changes in regional transport. The SLP and 500 hPa GPH over East Asia and Western Pacific
222 similar to those during the severe polluted months in both SCB and PRD have increased (2000-
223 2019 versus 1980-1999) (Figure 8), together with the more frequent hot and dry conditions
224 (Figure 7), leading to the increases in severe O₃ pollution in SCB and PRD during 1980–2019.

225 Many studies have reported that future climate change will have significant influences
226 on O₃ pollution in China through changing meteorological factors (e.g., Li et al., 2023; Wang
227 et al., 2022). Here, the frequencies of extreme months with high T_{2m} and low RH and the
228 frequencies of extreme months with SLP and 500 hPa GPH that have moderate to high
229 correlation to those in the polluted months in the four regions of China, under the sustainable
230 (SSP1-2.6) and high forcing (SSP5-8.5) scenarios during 2021–2100 from CMIP6 multi-model
231 results, are presented in Figures 9 and 10, respectively. The frequencies of months with
232 anomalous high temperature show obvious upward trends in both SSP1-2.6 and SSP5-8.5
233 scenarios over the four regions, and the increasing trends in SSP5-8.5 are much more
234 significant than in SSP1-2.6. Frequencies of low RH months show downward trends in NCP,
235 YRD and SCB, especially under SSP5-8.5, while there is an upward trend in PRD. Note that
236 the trends in frequencies of low RH months are much less significant than in high temperature
237 months. The frequencies of extreme months with SLP and 500 hPa GPH that are similar to
238 those in the severe O₃ pollution months in the four regions do not show significant trends in
239 the SSPs. Hence, the future climate change may aggregate O₃ pollution in China by enhancing



240 the chemical production related to temperature increases. The O₃ pollution exacerbation is
241 projected to be less significant in the sustainable scenario due to the moderate temperature
242 increase than in the high forcing scenario, suggesting that the sustainable scenario is the
243 optimal path to retaining clean air in China. High anthropogenic radiative forcing will not only
244 lead to slow economic growth and climate warming, but also result in the environmental
245 pollution.

246 **4. Conclusions**

247 O₃ pollution harms ecosystems and human health. In recent years, near-surface O₃
248 concentrations in many regions of China have been increasing considerably. Base on
249 observational O₃ data, ERA5 reanalysis data and GEOS-Chem model simulations,
250 meteorological characteristics conducive to severe O₃ pollution in different regions of China
251 are investigated in this study. Contributions from various chemical and physical processes
252 inducing O₃ pollution are quantified using an integrated process rate (IPR) analysis method.
253 Furthermore, historical changes and future trends of meteorological conditions leading to
254 severe O₃ pollution in China are explored based on the meteorological reanalysis and CMIP6
255 multi-model future predictions, which is of great implication for the mitigation and prevention
256 of O₃ pollution over China.

257 In this study, June 2018, July 2017, July 2015 and September 2019 are identified as the
258 most severe O₃ pollution months influenced by meteorological factors over NCP, YRD, SCB
259 and PRD, respectively. Severe O₃ pollution in June 2018 over NCP and in July 2017 over YRD
260 is mainly due to enhanced chemical production related to hot and dry conditions. The chemical
261 production of O₃ in the severe polluted months over NCP and YRD are 2.36 Gg day⁻¹ and 2.38



262 Gg day⁻¹, respectively, higher than the climatological averages. Different from NCP and YRD,
263 regional transport is the main process leading to the high O₃ concentration in SCB and PRD
264 during the respective severely polluted months, which contributes to the rate of increase in O₃
265 mass by 5.10 and 6.67 Gg day⁻¹, respectively, over SCB and PRD. During the severely polluted
266 months, related to large-scale circulation patterns, anomalous northerly winds transport more
267 O₃ into SCB from north, and anomalous northeasterly winds enhance the O₃ transport from the
268 north and east into PRD.

269 Over the last four decades (2000-2019 versus 1980-1999), the frequencies of high
270 temperature and low RH increased, indicating that O₃ pollution in both NCP and YRD has
271 become more frequent under the historical climate change. In SCB and PRD, the occurrence
272 of atmospheric circulation patterns similar to those during the polluted months in both SCB
273 and PRD has increased, together with the more frequent hot and dry conditions, leading to the
274 increases in severe O₃ pollution in SCB and PRD during 1980–2019. In the future (by 2100),
275 the frequencies of months with anomalous high temperature show obvious upward trends in
276 both sustainable (SSP1-2.6) and high forcing (SSP5-8.5) scenarios over the four regions, and
277 the increasing trends in SSP5-8.5 are much more significant than in SSP1-2.6. This suggests
278 that high anthropogenic radiative forcing will not only lead to slow economic growth and
279 climate warming, but also likely result in environmental pollution issues. The sustainable
280 scenario is the optimal path to retaining clean air in China.

281



282 **References**

- 283 Ainsworth, E. A., Yendrek, C. R., Sitch, S., Collins, W. J., and Emberson, L. D.: The Effects of
284 Tropospheric Ozone on Net Primary Productivity and Implications for Climate Change,
285 *Annu. Rev. Plant Biol.*, 63, 637-661, [https://doi.org/10.1146/annurev-arplant-042110-](https://doi.org/10.1146/annurev-arplant-042110-103829)
286 [103829](https://doi.org/10.1146/annurev-arplant-042110-103829), 2012.
- 287
- 288 Cheng, N., Li, R., Xu, C., Chen, Z., Chen, D., Meng, F., Cheng, B., Ma, Z., Zhuang, Y., He, B.,
289 and Gao, B.: Ground ozone variations at an urban and a rural station in Beijing from 2006
290 to 2017: trend, meteorological influences and formation regimes, *J. Clean. Prod.*, 235, 11–
291 20, <https://doi.org/10.1016/j.jclepro.2019.06.204>, 2019.
- 292
- 293 Coates, J., Mar, K. A., Ojha, N., and Butler, T. M.: The influence of temperature on ozone
294 production under varying NO_x conditions—a modelling study, *Atmos. Chem. Phys.*, 16,
295 11601-11615, <https://doi.org/10.5194/acp-16-11601-2016>, 2016.
- 296
- 297 Dang, R., Liao, H., and Fu, Y.: Quantifying the anthropogenic and meteorological influences
298 on summertime surface ozone in China over 2012-2017, *Sci. Total Environ.*, 754, 142394,
299 <https://doi.org/10.1016/j.scitotenv.2020.142394>, 2021.
- 300
- 301 Dong, Y., Li, J., Guo, J., Jiang, Z., Chu, Y., Chang, L., Yang, Y., and Liao, H.: The impact of
302 synoptic patterns on summertime ozone pollution in the North China Plain, *Sci. Total*
303 *Environ.*, 735, 139559, <https://doi.org/10.1016/j.scitotenv.2020.139559>, 2020.
- 304
- 305 Ebi, K. L. and McGregor, G.: Climate change, tropospheric O₃ and particulate matter, and
306 health impacts, *Environ. Health Perspect.*, 116, 1449-1455,
307 <https://doi.org/10.1289/ehp.11463>, 2008.
- 308
- 309 Finlayson-Pitts, B. J., and Pitts, J. N.: Tropospheric air pollution: Ozone, airborne toxics,
310 polycyclic aromatic hydrocarbons, and particles, *Science*, 276, 1045-1052,
311 <https://doi.org/10.1126/science.276.5315.1045>, 1997.
- 312
- 313 Fleming, Z. L., Doherty, R. M., Von Schneidemesser, E., Malley, C. S., Cooper, O. R., Pinto,
314 J. P., Colette, A., Xu, X. B., Simpson, D., Schultz, M. G., Lefohn, A. S., Hamad, S., Moolla,
315 R., Solberg, S., and Feng, Z. Z.: Tropospheric Ozone Assessment Report: Present-day
316 ozone distribution and trends relevant to human health, *Elementa-Sci. Anthropol.*, 6, 12,
317 <https://doi.org/10.1525/elementa.273>, 2018.
- 318
- 319 Fu, T.-M., and Tian, H.: Climate change penalty to ozone air quality: Review of current
320 understandings and knowledge gaps, *Curr. Pollution Rep.*, 5, 159–171,
321 <https://doi.org/10.1007/s40726-019-00115-6>, 2019.
- 322
- 323 Guenther, A. B., Jiang, X., Heald, C. L., Sakulyanontvittaya, T., Duhl, T., Emmons, L. K., and
324 Wang, X.: The Model of Emissions of Gases and Aerosols from Nature version 2.1
325 (MEGAN2.1): an extended and updated framework for modeling biogenic emissions,



- 326 Geosci. Model Dev., 5, 1471–1492, <https://doi.org/10.5194/gmd-5-1471-2012>, 2012.
- 327
- 328 Gong, C., and Liao, H.: A typical weather pattern for ozone pollution events in North China,
329 Atmos. Chem. Phys., 19, 13725–13740, <https://doi.org/10.5194/acp-19-13725-2019>,
330 2019.
- 331
- 332 Han, H., Liu, J., Shu, L., Wang, T. J., and Yuan, H.: Local and synoptic meteorological
333 influences on daily variability in summertime surface ozone in eastern China, Atmos.
334 Chem. Phys., 20, 203–222, <https://doi.org/10.5194/acp-20-203-2020>, 2020.
- 335
- 336 Hoesly, R. M., Smith, S. J., Feng, L., Klimont, Z., Janssens-Maenhout, G., Pitkanen, T., Seibert,
337 J. J., Vu, L., Andres, R. J., Bolt, R. M., Bond, T. C., Dawidowski, L., Kholod, N.,
338 Kurokawa, J. I., Li, M., Liu, L., Lu, Z., Moura, M. C. P., O’Rourke, P. R., and Zhang, Q.:
339 Historical (1750–2014) anthropogenic emissions of reactive gases and aerosols from the
340 Community Emissions Data System (CEDS), Geosci. Model Dev., 11, 369–408,
341 <https://doi.org/10.5194/gmd-11-369-2018>, 2018.
- 342
- 343 Hudman, R. C., Moore, N. E., Mebust, A. K., Martin, R. V., Russell, A. R., Valin, L. C., and
344 Cohen, R. C.: Steps towards a mechanistic model of global soil nitric oxide emissions:
345 implementation and space based-constraints, Atmos. Chem. Phys., 12, 7779–7795,
346 <https://doi.org/10.5194/acp-12-7779-2012>, 2012.
- 347
- 348 Jiang, Z., Li, J., Lu, X., Gong, C., Zhang, L., and Liao, H.: Impact of western Pacific subtropical
349 high on ozone pollution over eastern China, Atmos. Chem. Phys., 21, 2601–2613,
350 <https://doi.org/10.5194/acp-21-2601-2021>, 2021.
- 351
- 352 Le, T., Wang, Y., Liu, L., Yang, J., Yung, Y., Li, G., and Seinfeld, J. H.: Unexpected air pollution
353 with marked emission reductions during the COVID-19 outbreak in China, Science, 369,
354 702–706, <https://doi.org/10.1126/science.abb7431>, 2020.
- 355
- 356 Li, H., Yang, Y., Jin, J., Wang, H., Li, K., Wang, P., and Liao, H.: Climate-driven deterioration
357 of future ozone pollution in Asia predicted by machine learning with multi-source data,
358 Atmos. Chem. Phys., 23, 1131–1145, <https://doi.org/10.5194/acp-23-1131-2023>, 2023.
- 359
- 360 Li, K., Jacob, D. J., Liao, H., Shen, L., Zhang, Q., and Bates, K. H.: Anthropogenic drivers of
361 2013–2017 trends in summer surface ozone in China, P. Natl. Acad. Sci. USA, 116, 422–
362 427, <https://doi.org/10.1073/pnas.1812168116>, 2019.
- 363
- 364 Li, K., Jacob, D. J., Shen, L., Lu, X., De Smedt, I., and Liao, H.: Increases in surface ozone
365 pollution in China from 2013 to 2019: anthropogenic and meteorological influences,
366 Atmos. Chem. Phys., 20, 11423–11433, <https://doi.org/10.5194/acp-20-11423-2020>, 2020.
- 367
- 368 Lin, J.-T., and McElroy, M. B.: Impacts of boundary layer mixing on pollutant vertical profiles
369 in the lower troposphere: Implications to satellite remote sensing, Atmos. Environ., 44,



- 370 1726–1739, <https://doi.org/10.1016/j.atmosenv.2010.02.009>, 2010.
- 371
- 372 Liu, H., Liu, S., Xue, B., Lv, Z., Meng, Z., Yang, X., Xue, T., Yu, Q., and He, K.: Ground-level
373 ozone pollution and its health impacts in China, *Atmos. Environ.*, 173, 223–230,
374 <https://doi.org/10.1016/j.atmosenv.2017.11.014>, 2018.
- 375
- 376 Liu, Y., and Wang, T.: Worsening urban ozone pollution in China from 2013 to 2017–Part 1:
377 The complex and varying roles of meteorology, *Atmos. Chem. Phys.*, 20, 6305–6321,
378 <https://doi.org/10.5194/acp-20-6305-2020>, 2020.
- 379
- 380 Lu, X., Hong, J., Zhang, L., Cooper, O. R., Schultz, M. G., Xu, X., Wang, T., Gao, M., Zhao,
381 Y., and Zhang, Y.: Severe Surface Ozone Pollution in China: A Global Perspective,
382 *Environ. Sci. Technol. Lett.*, 5, 487–494, <https://doi.org/10.1021/acs.estlett.8b00366>,
383 2018.
- 384
- 385 Lu, X., Zhang, L., Chen, Y., Zhou, M., Zheng, B., Li, K., Liu, Y., Lin, J., Fu, T.-M., and Zhang,
386 Q.: Exploring 2016–2017 surface ozone pollution over China: source contributions and
387 meteorological influences, *Atmos. Chem. Phys.*, 19, 8339–8361,
388 <https://doi.org/10.5194/acp-19-8339-2019>, 2019.
- 389
- 390 Lu, X., Zhang, L., Wang, X., Gao, M., Li, K., Zhang, Y., Yue, X., and Zhang, Y.: Rapid increases
391 in warm-season surface ozone and resulting health impact over China since 2013, *Environ.*
392 *Sci. Technol. Lett.*, 7, 240–247, <https://doi.org/10.1021/acs.estlett.0c00171>, 2020.
- 393
- 394 Maji, K. J., Ye, W.-F., Arora, M., and Nagendra, S. M. S.: Ozone pollution in Chinese cities:
395 Assessment of seasonal variation, health effects and economic burden, *Environ. Pollut.*,
396 247, 792–801, <https://doi.org/10.1016/j.envpol.2019.01.049>, 2019.
- 397
- 398 Mao, J., Paulot, F., Jacob, D. J., Cohen, R. C., Crouse, J. D., Wennberg, P. O., Keller, C. A.,
399 Hudman, R. C., Barkley, M. P., and Horowitz, L. W.: Ozone and organic nitrates over the
400 eastern United States: Sensitivity to isoprene chemistry, *J. Geophys. Res. Atmos.*, 118,
401 11256–11268, <https://doi.org/10.1002/jgrd.50817>, 2013.
- 402
- 403 McLinden, C. A., Olsen, S. C., Hannegan, B., Wild, O., Prather, M. J., and Sundet, J.:
404 Stratospheric ozone in 3-D models: A simple chemistry and the cross-tropopause flux, *J.*
405 *Geophys. Res.*, 105, 14653–14665, <https://doi.org/10.1029/2000jd900124>, 2000.
- 406
- 407 Mills, G., Sharps, K., Simpson, D., Pleijel, H., Broberg, M., Uddling, J., Jaramillo, F., Davies,
408 W. J., Dentener, F., Van den Berg, M., Agrawal, M., Agrawal, S. B., Ainsworth, E. A.,
409 Buker, P., Emberson, L., Feng, Z., Harmens, H., Hayes, F., Kobayashi, K., Paoletti, E.,
410 and Van Dingenen, R.: Ozone pollution will compromise efforts to increase global wheat
411 production, *Glob. Chang. Biol.*, 24, 3560–3574, <https://doi.org/10.1111/gcb.14157>, 2018.
- 412
- 413 Mott, J. A., Mannino, D. M., Alverson, C. J., Kiyu, A., Hashim, J., Lee, T., Falter, K., Redd, S.



- 414 C.: Cardiorespiratory hospitalizations associated with smoke exposure during the 1997
415 southeast Asian forest fires, *Int. J. Hyg. Environ. Health.*, 208, 75–85,
416 <https://doi.org/10.1016/j.ijheh.2005.01.018>, 2005.
417
- 418 Ni, R., Lin, J., Yan, Y., and Lin, W.: Foreign and domestic contributions to springtime ozone
419 over China, *Atmos. Chem. Phys.*, 18, 11447–11469, <https://doi.org/10.5194/acp-18-11447-2018>, 2018.
420
421
- 422 Ott, L. E., Pickering, K. E., Stenchikov, G. L., Allen, D. J., DeCaria, A. J., Ridley, B., Lin, R.-
423 F., Lang, S., and Tao, W.-K.: Production of lightning NO_x and its vertical distribution
424 calculated from three-dimensional cloud-scale chemical transport model simulations, *J. Geophys. Res.*, 115, D04301, <https://doi.org/10.1029/2009JD011880>, 2010.
425
426
- 427 Peterson, J. T., and Flowers, E. C.: Interactions between air pollution and solar radiation, *Sol. Energy*, 19, 23–32, [https://doi.org/10.1016/0038-092X\(77\)90085-8](https://doi.org/10.1016/0038-092X(77)90085-8), 1977.
428
429
- 430 Pye, H. O., Liao, H., Wu, S., Mickley, L. J., Jacob, D. J., Henze, D. K., and Seinfeld, J. H.:
431 Effect of changes in climate and emissions on future sulfate-nitrate-mmonium aerosol
432 levels in the United States, *J. Geophys. Res.*, 114, D01205, <https://doi.org/10.1029/2008JD010701>, 2009.
433
434
- 435 Sherwen, T., Schmidt, J. A., Evans, M. J., Carpenter, L. J., Großmann, K., Eastham, S. D.,
436 Jacob, D. J., Dix, B., Koenig, T. K., Sinreich, R., Ortega, I., Volkamer, R., Saiz-Lopez, A.,
437 Prados-Roman, C., Mahajan, A. S., and Ordóñez, C.: Global impacts of tropospheric
438 halogens (Cl, Br, I) on oxidants and composition in GEOS-Chem, *Atmos. Chem. Phys.*,
439 16, 12239–12271, <https://doi.org/10.5194/acp-16-12239-2016>, 2016.
440
- 441 Shu, L., Wang, T., Han, H., Xie, M., Chen, P., Li, M., and Wu, H.: Summertime ozone pollution
442 in the Yangtze River Delta of eastern China during 2013–2017: synoptic impacts and
443 source apportionment, *Environ. Pollut.*, 257, 113631, <https://doi.org/10.1016/j.envpol.2019.113631>, 2020
444
445
- 446 Sillman, S.: The relation between ozone, NO_x and hydrocarbons in urban and polluted rural
447 environments, *Atmos. Environ.*, 33, 1821–1845, [https://doi.org/10.1016/s1352-2310\(98\)00345-8](https://doi.org/10.1016/s1352-2310(98)00345-8), 1999.
448
449
- 450 Silver, B., Reddington, C. L., Arnold, S. R., and Spracklen, D. V.: Substantial changes in air
451 pollution across China during 2015–2017, *Environ. Res. Lett.*, 13, 114012, <https://doi.org/10.1088/1748-9326/aae718>, 2018.
452
453
- 454 Sekiya, T., and Sudo, K.: Roles of transport and chemistry processes in global ozone change
455 on interannual and multidecadal time scales, *J. Geophys. Res. Atmos.*, 119, 4903–4921,
456 <https://doi.org/10.1002/2013JD020838>, 2014.
457



- 458 van der Werf, G. R., Randerson, J. T., Giglio, L., van Leeuwen, T. T., Chen, Y., Rogers, B. M.,
459 Mu, M., van Marle, M. J. E., Morton, D. C., Collatz, G. J., Yokelson, R. J., and Kasibhatla,
460 P. S.: Global fire emissions estimates during 1997–2016, *Earth Syst. Sci. Data*, 9, 697–
461 720, <https://doi.org/10.5194/essd-9-697-2017>, 2017.
- 462
- 463 Verstraeten, W. W., Neu, J. L., Williams, J. E., Bowman, K. W., Worden, J. R., and Boersma,
464 K. F.: Rapid increases in tropospheric ozone production and export from China, *Nat.*
465 *Geosci.*, 8, 690–695, <https://doi.org/10.1038/ngeo2493>, 2015.
- 466
- 467 Wang, P., Yang, Y., Li, H., Chen, L., Dang, R., Xue, D., Li, B., Tang, J., Leung, L. R., and Liao,
468 H.: North China Plain as a hot spot of ozone pollution exacerbated by extreme high
469 temperatures, *Atmos. Chem. Phys.*, 22, 4705–4719, [https://doi.org/10.5194/acp-22-4705-](https://doi.org/10.5194/acp-22-4705-2022)
470 2022, 2022.
- 471
- 472 Wang, T., Xue, L., Brimblecombe, P., Lam, Y. F., Li, L., and Zhang, L.: Ozone pollution in
473 China: A review of concentrations, meteorological influences, chemical precursors, and
474 effects, *Sci. Total Environ.*, 575, 1582–1596,
475 <https://doi.org/10.1016/j.scitotenv.2016.10.081>, 2017.
- 476
- 477 Xu, J., Ma, J. Z., Zhang, X. L., Xu, X. B., Xu, X. F., Lin, W. L., Wang, Y., Meng, W., and Ma,
478 Z. Q.: Measurements of ozone and its precursors in Beijing during summertime: impact
479 of urban plumes on ozone pollution in downwind rural areas, *Atmos. Chem. Phys.*, 11,
480 12241–12252, <https://doi.org/10.5194/acp-11-12241-2011>, 2011.
- 481
- 482 Yang, Y., Liao, H., and Li, J.: Impacts of the East Asian summer monsoon on interannual
483 variations of summertime surface-layer ozone concentrations over China, *Atmos. Chem.*
484 *Phys.*, 14, 6867–6880, <http://doi:10.5194/acp-14-6867-2014>, 2014.
- 485
- 486 Yang, Y., Li, M., Wang, H., Li, H., Wang, P., Li, K., Gao, M., and Liao, H.: ENSO modulation
487 of summertime tropospheric ozone over China, *Environ. Res. Lett.*, 17, 034020,
488 <https://doi.org/10.1088/1748-9326/ac54cd>, 2022.
- 489
- 490 Yin, Z., Cao, B., and Wang, H.: Dominant patterns of summer ozone pollution in eastern China
491 and associated atmospheric circulations, *Atmos. Chem. Phys.*, 19, 13933–13943,
492 <https://doi.org/10.5194/acp-19-13933-2019>, 2019.
- 493
- 494 Zhang, X., Zhao, L., Cheng, M., Wu, X., and Chen, D.: Urban ozone sink inferred from surface
495 measurements in China, *J. Clean. Prod.*, 253, 119881,
496 <https://doi.org/10.1016/j.jclepro.2019.119881>, 2020.
- 497
- 498 Zhang, H., Wang, Y., Hu, J., Ying, Q., and Hu, X.-M.: Relationships between meteorological
499 parameters and criteria air pollutants in three megacities in China, *Environ. Res.*, 140,
500 242–254, <https://doi.org/10.1016/j.envres.2015.04.004>, 2015.
- 501



- 502 Zhao, Y., Zhang, K., Xu, X., Shen, H., Zhu, X., Zhang, Y., Hu, Y., and Shen, G.: Substantial
503 changes in nitrogen dioxide and ozone after excluding meteorological impacts during the
504 COVID-19 outbreak in mainland China, *Environ. Sci. Technol. Lett.*, 7, 402–408,
505 <https://doi.org/10.1021/acs.estlett.0c00304>, 2020.
506
- 507 Zhao, Z., and Wang, Y.: Influence of the West Pacific subtropical high on surface ozone daily
508 variability in summertime over eastern China, *Atmos. Environ.*, 170, 197–204,
509 <https://doi.org/10.1016/j.atmosenv.2017.09.024>, 2017.
510
- 511 Zhou, D., Ding, A., Mao, H., Fu, C., Wang, T., Chan, L. Y., Ding, K., Zhang, Y., Liu, J., and
512 Lu, A.: Impacts of the East Asian monsoon on lower tropospheric ozone over coastal
513 South China, *Environ. Res. Lett.*, 8, 044011, [https://doi.org/10.1088/1748-](https://doi.org/10.1088/1748-9326/8/4/044011)
514 [9326/8/4/044011](https://doi.org/10.1088/1748-9326/8/4/044011), 2013.
515



516 **Code and data availability.** The GEOS-Chem model is available at
517 <https://zenodo.org/record/3974569#.YTD81NMzagR> (last access: June 2023). O₃ observations
518 over China can be obtained at <https://quotsoft.net/air> (last access: June 2023). ERA5 reanalysis
519 data can be downloaded at [https://www.ecmwf.int/en/forecasts/datasets/reanalysis-](https://www.ecmwf.int/en/forecasts/datasets/reanalysis-datasets/era5)
520 [datasets/era5](https://www.ecmwf.int/en/forecasts/datasets/reanalysis-datasets/era5) (last access: June 2023). The multi-model simulations of the Coupled Model
521 Intercomparison Project Phase 6 (CMIP6) are from <https://esgf-node.llnl.gov/search/cmip6/>
522 (last access: June 2023).

523 **Author contribution.** YY designed the research; YY and YZ performed simulations and
524 analyzed the data. All authors including HW, LH, PW, and HL discussed the results and wrote
525 the paper.

526 **Competing interests.** At least one of the (co-)authors is a member of the editorial board of
527 Atmospheric Chemistry and Physics.

528 **Acknowledgments.** HW acknowledges the support by the U.S. Department of Energy (DOE),
529 Office of Science, Office of Biological and Environmental Research (BER), as part of the Earth
530 and Environmental System Modeling program. The Pacific Northwest National Laboratory
531 (PNNL) is operated for DOE by the Battelle Memorial Institute under contract DE-AC05-
532 76RLO1830.

533 **Financial support.** This study was supported by the National Natural Science Foundation of
534 China (grant 42293323), and the National Key Research and Development Program of China
535 (grant 2020YFA0607803), Jiangsu Science Fund for Distinguished Young Scholars (grant
536 BK20211541), and the Jiangsu Science Fund for Carbon Neutrality (grant BK20220031).



537 **Table 1.** Anomalies in net rate of changes in tropospheric O₃ mass (Gg day⁻¹) over NCP (115°–
538 120°E, 38°–44°N), YRD (120°–125°E, 28°–32°N), SCB (102.5°–105°E, 30°–32°N) and PRD
539 (110°–115°E, 22°–26°N) due to physical and chemical processes in the most polluted months
540 (June 2018, July 2017, July 2015 and September 2019, respectively) relative to the same
541 months averaged during 1981–2019.

542

	Beijing	Shanghai	Chengdu	Guangzhou
Chemical reaction	2.36	2.38	-2.80	-1.52
Horizontal transport	1.58	-1.18	5.10	6.67
Diffusion and dry deposition	0.29	0.24	-0.73	-0.93

543

544

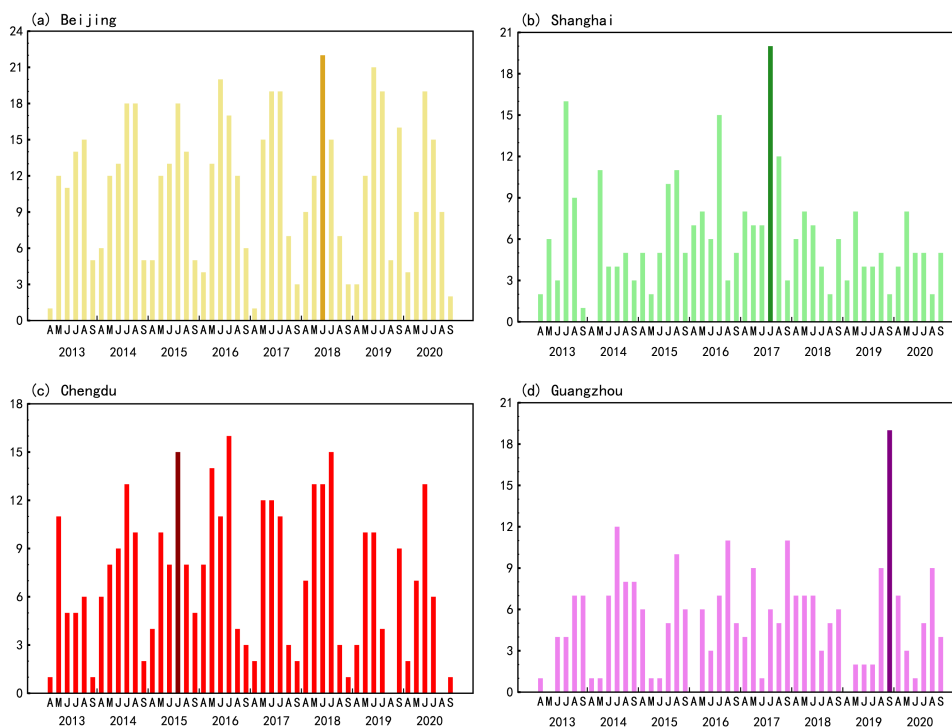


545 **Table 2.** Horizontal mass transport (T_g) of O_3 from the surface to 500 hPa over NCP (115°–
 546 120°E, 38°–44°N), YRD (120°–125°E, 28°–32°N), SCB (102.5°–105°E, 30°–32°N) and PRD
 547 (110°–115°E, 22°–26°N) areas in the severe polluted months (June 2018, July 2017, July 2015
 548 and September 2019, respectively) and averaged over the same months of a year during 1981–
 549 2019, as well as their differences. Positive values indicate incoming fluxes and negative values
 550 indicate outgoing fluxes.
 551

	Polluted month	Average	Anomalies
	NCP		
North	4.43	2.62	1.80
South	-2.22	-1.42	-0.81
East	-12.30	-11.31	-0.99
West	11.83	11.20	0.62
	YRD		
North	-4.13	-3.88	-0.25
South	3.58	3.20	0.37
East	-2.05	-3.90	1.85
West	2.03	4.04	-2.01
	SCB		
North	4.15	0.13	4.02
South	-2.30	0.48	-2.78
East	-1.10	-1.15	0.05
West	1.73	1.84	-0.11
	PRD		
North	2.70	0.72	1.97
South	-2.87	-0.90	-1.96
East	2.24	1.15	1.09
West	-2.32	-1.55	-0.76

552

553



554

555

556

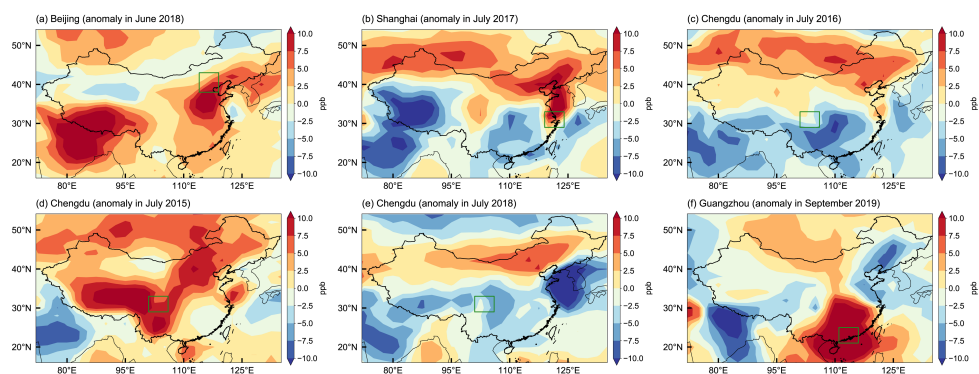
557

558

559

560

Figure 1. Time series of frequencies of severe O₃ pollution days (defined by daily maximum of 8-h average ozone (MDA8-O₃) concentration greater than 160 μg m⁻³) in Beijing, Shanghai, Chengdu and Guangzhou (a–d) from April to September during 2013–2020. The dark-colored bars represent the most severe month (second most for Chengdu) that has the highest frequency of O₃ pollution days for the individual cities.



561

562

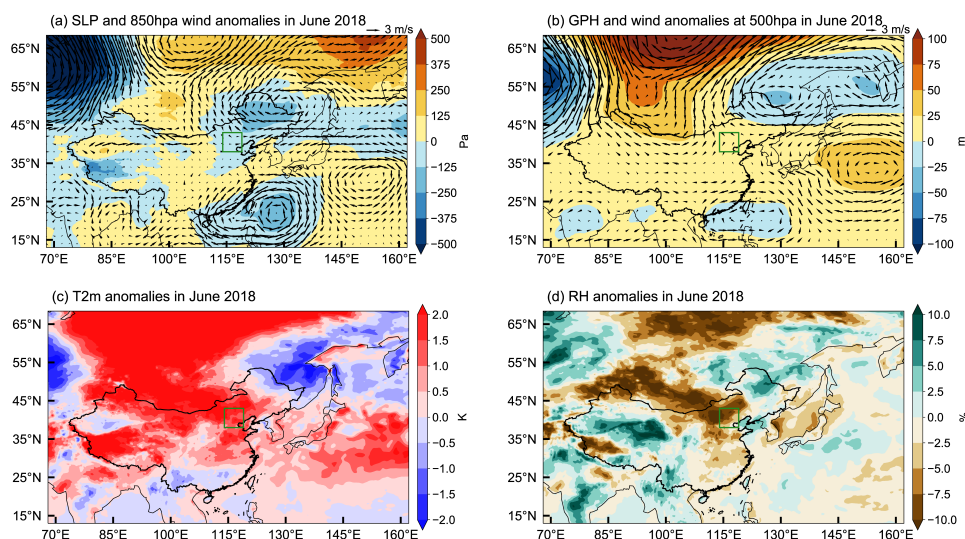
563

564

565

566

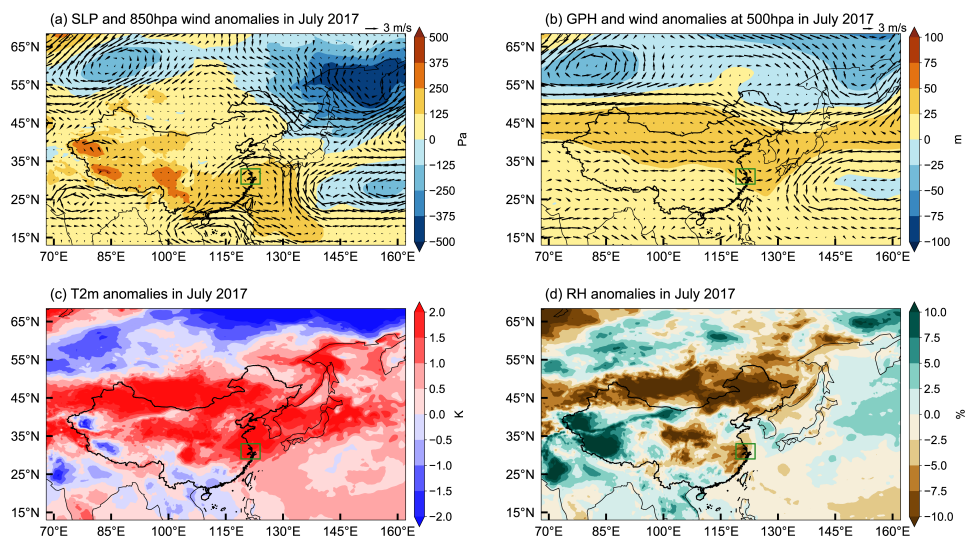
Figure 2. Spatial distribution of monthly O₃ concentration anomalies (part per billion, ppb) in June 2018 (a), July 2017 (b), July 2016 (c), July 2015 (d), July 2018 (e) and September 2019 (f), simulated in the GEOS-Chem model. The green boxes mark NCP (a), YRD (b), SCB (c, d, e) and PRD (f). Anomalies are relative to the corresponding monthly averages over 1980–2019.



567

568 **Figure 3.** Anomalies in sea level pressure (SLP, Pa, shaded) and 1000 hPa winds (m s^{-1} , vector)
569 (a), geopotential height (GPH, m, shaded) and winds at 500 hPa (m s^{-1} , vector) (b), 2-meter air
570 temperature (T2m, K) (c) and surface relative humidity (RH, %) (d) in June 2018 relative to
571 the 40-year (1980–2019) monthly average for June. The green boxes mark NCP.

572



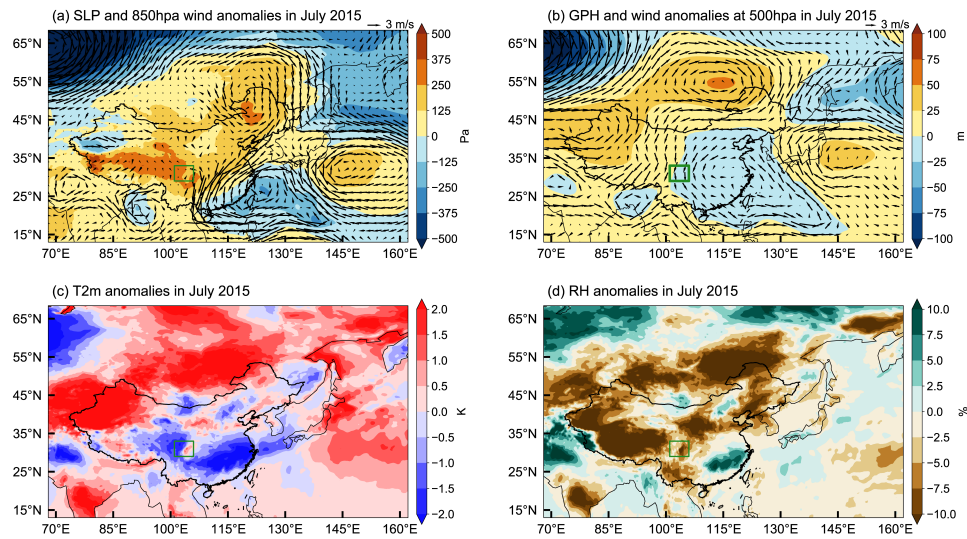
573

574

575

576

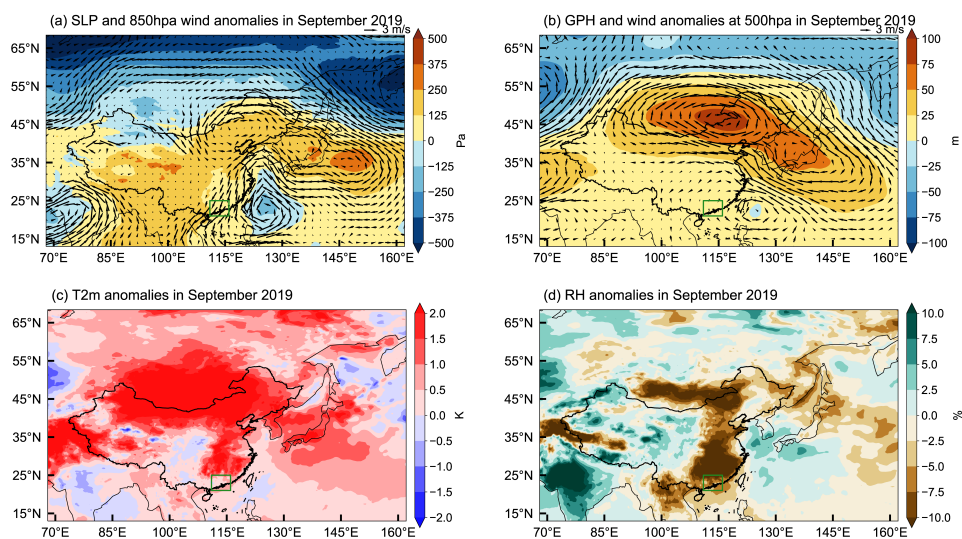
Figure 4. Same as Figure 3 but for the monthly anomalies in July 2017. The green boxes mark YRD.



577

578 **Figure 5.** Same as Figure 3 but for the monthly anomalies in July 2015. The green boxes mark
579 SCB.

580

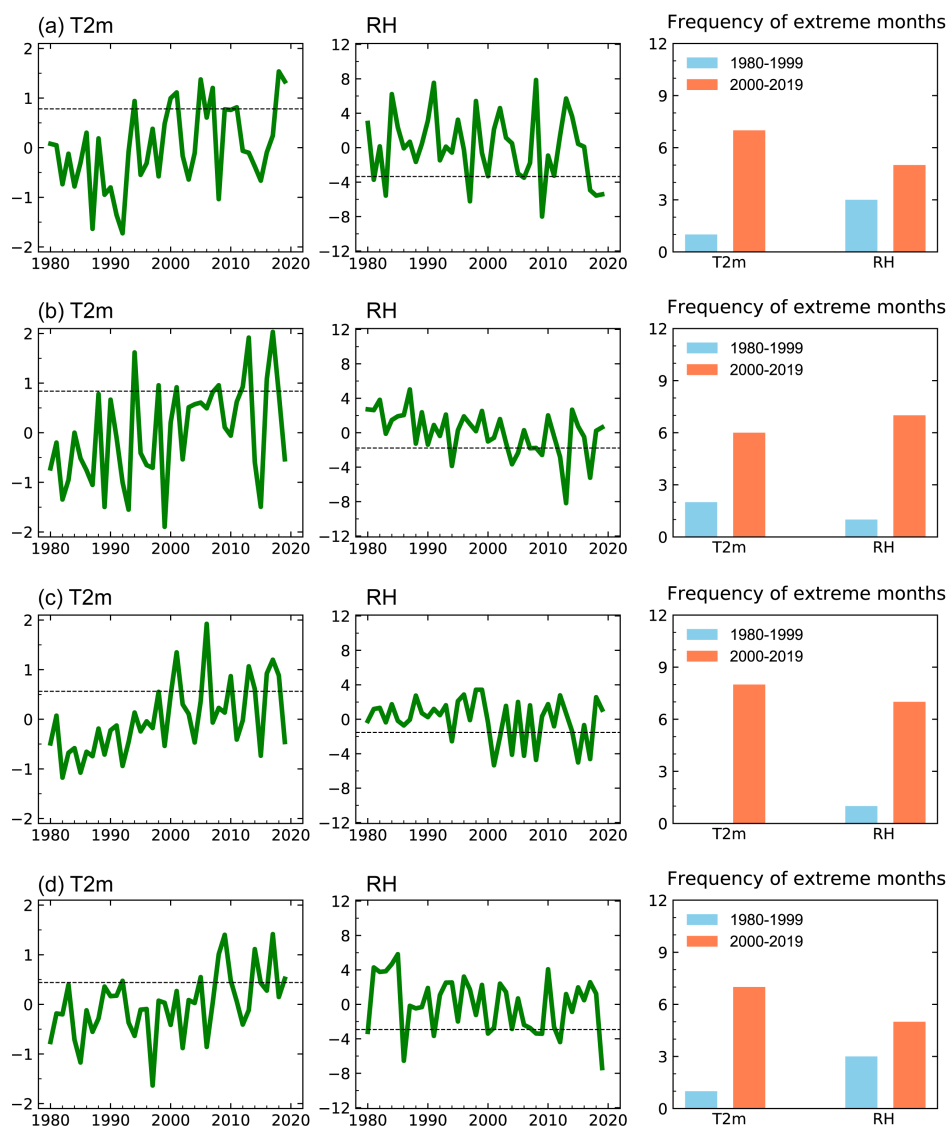


581

582

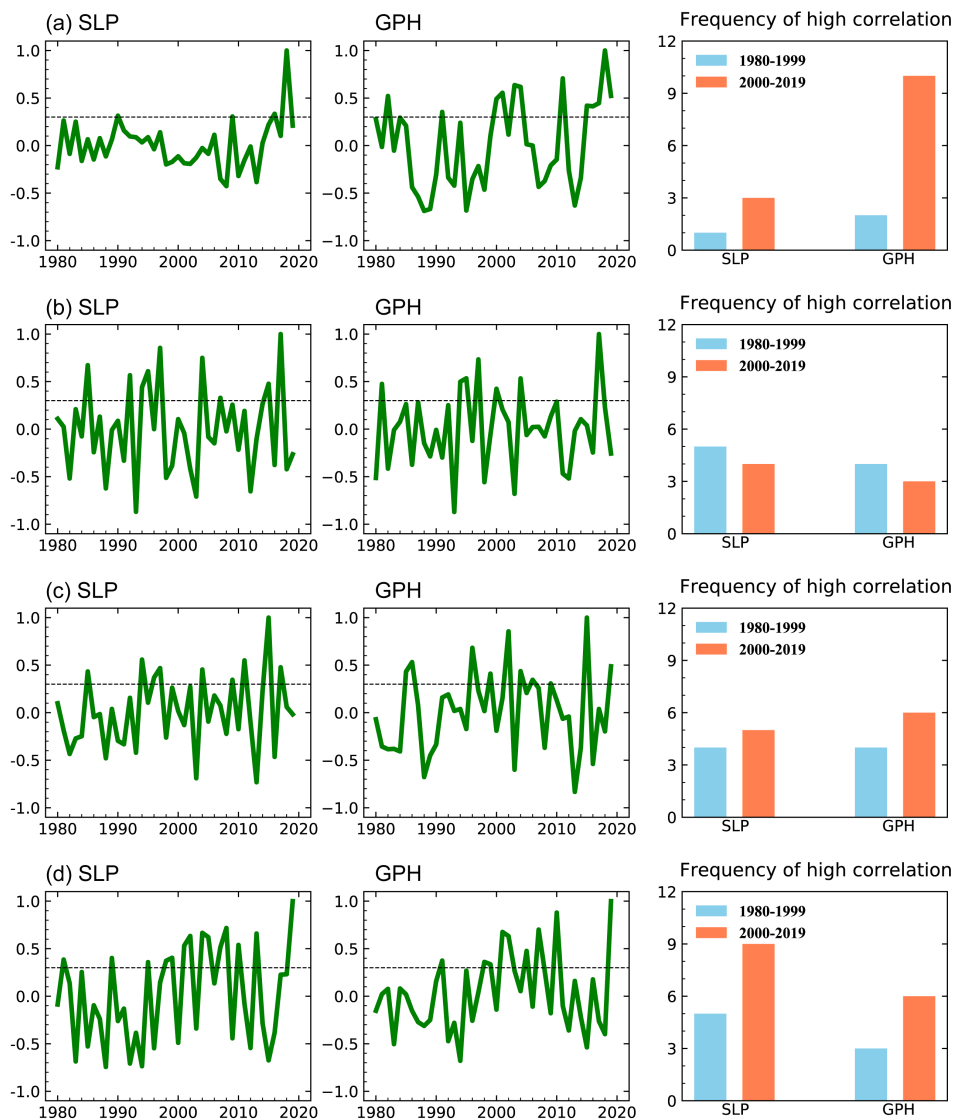
583

Figure 6. Same as Figure 3 but for the monthly anomalies in September 2019. The green boxes mark PRD.



584

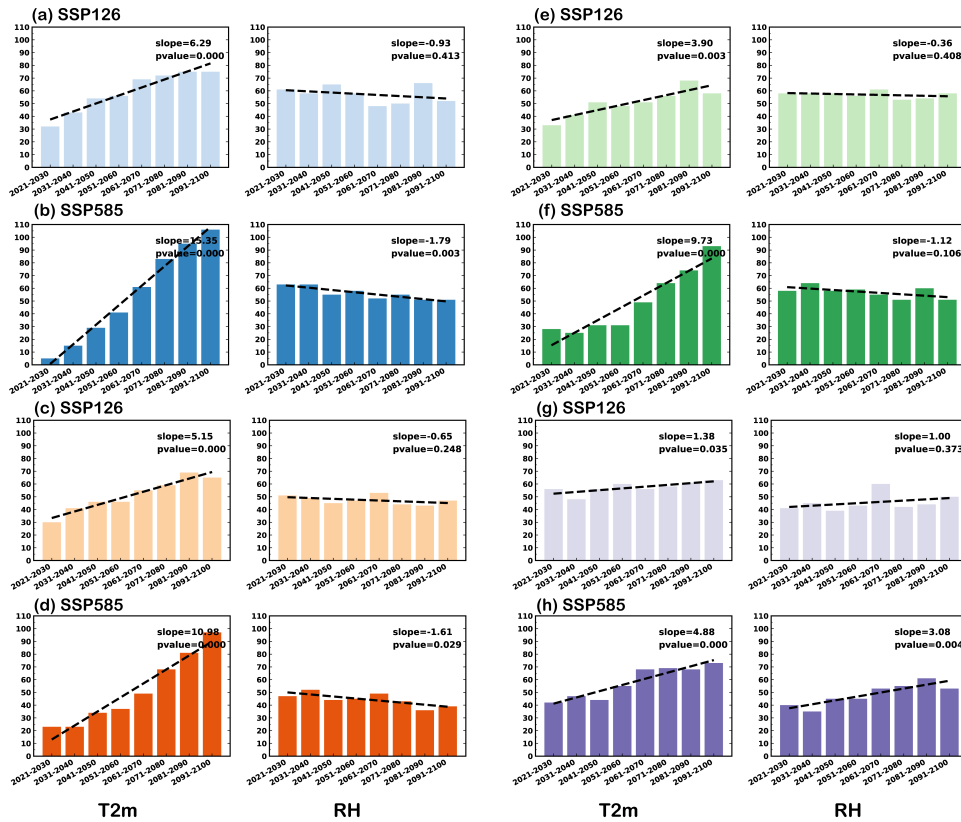
585 **Figure 7.** Time series of anomalies of T2m (K, left) and RH at 1000 hPa (% , middle) over (a)
 586 NCP (115°–120°E, 38°–44°N), (b) YRD (120°–125°E, 28°–32°N), (c) SCB (102.5°–105°E,
 587 30°–32°N) and (d) PRD (110°–115°E, 22°–26°N) in the most polluted months during 1980–
 588 2019. The dotted lines mark the 80th percentile of the distributions for T2m and 20th percentile
 589 for RH. The bar charts (right) represent the frequency of T2m above the 80th percentile and
 590 RH anomalies below the 20th percentile during 1980–1999 (blue) and 2000–2019 (orange).



591

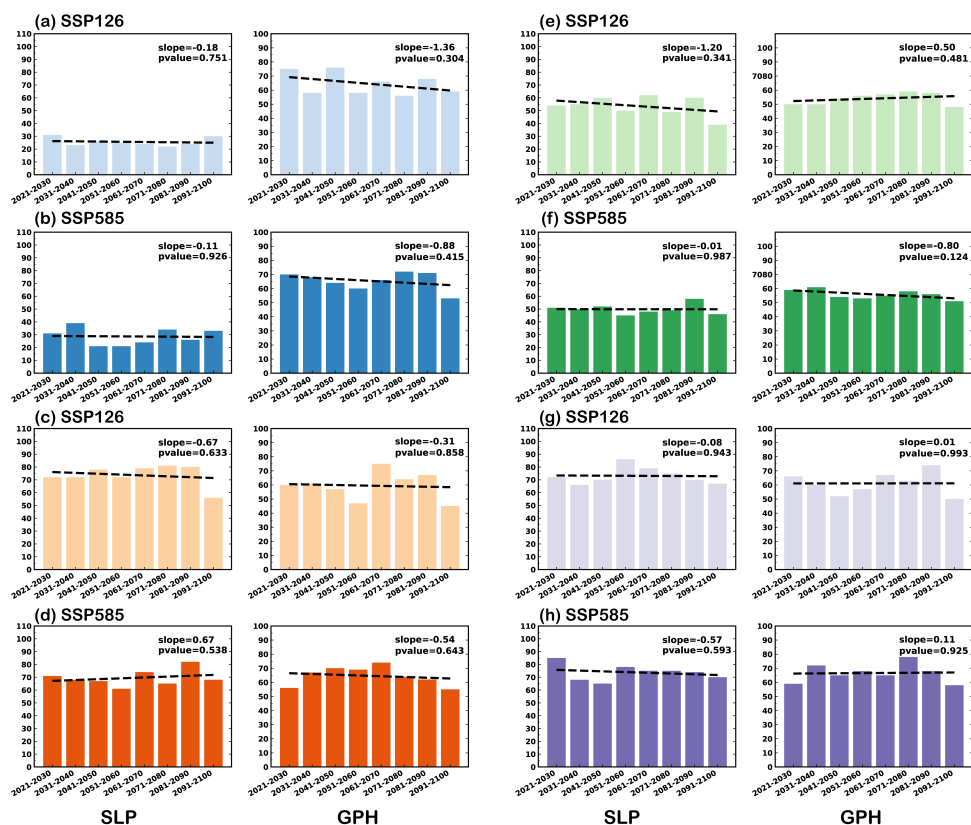
592 **Figure 8.** Time series of spatial correlation in SLP (left) and 500 hPa GPH (middle) anomalies
 593 over East Asia and Western Pacific (EAWP, 90°–160°E, 20°–60°N) in June 2018 (a), July 2017
 594 (b), July 2015 (c) and September 2019 (d) and those of each year during 1980–2019. The dotted
 595 lines mark the correlation coefficient of +0.3, which is used as a threshold to define “moderate
 596 to high correlation”. The bar chart (right) represents the frequency of SLP and 500 hPa GPH
 597 anomalies in the same months during 1980–1999 (blue) and 2000–2019 (orange) that have
 598 moderate to high correlation (>0.3) with those in June 2018, July 2017, July 2015 and
 599 September 2019.

600



601

602 **Figure 9.** Frequencies of extreme RH months with T2m or RH anomalies exceeding the 80th
 603 percentile or below the 20th percentile of the distributions over NCP (115°–120°E, 38°–44°N)
 604 (a, b), YRD (120°–125°E, 28°–32°N) (c, d), SCB (102.5°–105°E, 30°–32°N) (e, f) and PRD
 605 (110°–115°E, 22°–26°N) (g, h) in each 10-year interval during 2021–2100 under two SSPs
 606 future scenarios of 13 CMIP6 models. The two SSPs are SSP1-2.6 and SSP5-8.5. The slope
 607 and P values of the linear regression during 2021–2100 are shown in the upper right of each
 608 panel.



609

610 **Figure 10.** Frequencies of extreme months with SLP and 500 hPa GPH that have moderate to
 611 high correlation (>0.3) to those in June 2018 (a, b), July 2017 (c, d), July 2015 (e, f) and
 612 September 2019 (g, h) in each 10-year interval during 2021–2100 under two SSPs future
 613 scenarios of 13 CMIP6 models. The two SSPs are SSP1-2.6 and SSP5-8.5. The slope and P
 614 values of the linear regression during 2021–2100 are shown in the upper right of each panel.
 615 The linear trends of SLP and GPH in each model grid were removed before the correlation
 616 coefficient is calculated.